Interplay of 3*d*- and 5*d*-sublattice magnetism in the double perovskite substitution series $La_2Zn_{1-x}Co_xIrO_6$

M. Vogl,[1,*] L. T. Corredor,[1] T. Dey,[1,2] R. Morrow,[1] F. Scaravaggi,[1,3] A. U. B. Wolter,[1] S. Aswartham,[1,†] S. Wurmehl,[1,3] and B. Büchner[1,3]

[1]*Leibniz Institute for Solid State and Materials Research, D-01069 Dresden, Germany*
[2]*EP-VI, Electronic Correlations and Magnetism, University of Augsburg, D-86135 Augsburg, Germany*
[3]*Institut für Festkörperphysik, TU Dresden, D-01062 Dresden, Germany*

(Received 10 November 2017; revised manuscript received 15 December 2017; published 25 January 2018)

We report on the interplay of 3*d*- and 5*d*-sublattice magnetism in polycrystalline samples of the double perovskite substitution series $La_2Zn_{1-x}Co_xIrO_6$. Powder x-ray diffraction reveals no major structural changes within the series. In magnetization measurements, a gradual shift of the transition temperature from $T_N \approx 91$ K for the Co parent compound to $T_N \approx 8.7$ K for the Zn parent compound is observed. The data on the Zn-rich members of the substitution series indicate that this is accompanied by changing roles of the 3*d* sublattice of Co^{2+} and the strongly spin-orbit coupled 5*d*-sublattice of Ir^{4+} with its $j_{eff} = 1/2$ ground state, as a function of the Co/Zn ratio. Temperature-dependent specific-heat studies revealed a reduced magnetic entropy, pointing towards a large spin-orbit coupling and orbital contribution in the system.

DOI: 10.1103/PhysRevB.97.035155

I. INTRODUCTION

In recent years, transition metal oxides with 4*d* and 5*d* elements have drawn great interest due to their unique combination of crystal-field splitting, large spin-orbit coupling (SOC), and Coulomb repulsion [1–3]. The competition between these different energetic contributions can lead to exotic ground states such as Mott insulators, topological insulators, topological superconductors, and Weyl semimetals [2,4–7]. Iridates with Ir^{4+} states in particular have shown interesting features. The $j_{eff} = 1/2$ ground state, caused by the aforementioned interactions, has been the subject of many recent research activities, e.g., the search for unique magnetic phases such as quantum spin liquids [8–10].

Another intriguing field in which to study unique magnetic behavior has been perovskite-structure-type materials with the universal formula ABO_3. In general, the perovskite structure is built up by corner-sharing BO_6 octahedra. The *A* cations occupy the space in between the octahedra. Simple perovskite materials have received research interest mainly due to their intriguing multiferroic properties [11–14]. In the double perovskite structure, two different *B* cations are present, leading to the general formula $A_2BB'O_6$. An important aspect of the crystal structure is the *B*-site cation ordering. In the most common "rock-salt"-structure, BO_6 and $B'O_6$ octahedra are alternating, although compounds with layered or columnar order are also known [15]. As the most common *A* cations, e.g., La^{3+} and alkaline earth metal ions, are nonmagnetic, the magnetic properties of these materials are determined by the B/B' cations. In a "rock-salt"-ordered double perovskite, the *B* and *B'* sublattices can be viewed as two interpenetrating face-centered cubic (fcc) lattices. In this case, a multitude of different magnetic exchange interactions ranging from short-range nearest-neighbor (*B*-*B'*) or next-nearest-neighbor (*B*-B/B'-*B'*) interactions to long-range B/B'-sublattice orderings are possible. The interplay of these interactions can lead to a variety of unique magnetic ground states [16–25]. Another common feature in perovskites is the tilting of the octahedra [26,27]. As an effect, the strong deviation of the *B*-O-*B'* angle from 180° can lead to anisotropic exchange interactions, such as Dzyaloshinskii-Moriya interactions, allowing the formation of canted spin structures [28,29].

In this paper, we discuss the case of double perovskites with a 3*d* transition metal (Co^{2+}) on one *B* site and the strongly spin-orbit coupled 5*d* transition metal Ir^{4+} on the 2nd *B* position. Additional to its spin-contribution, Co^{2+} is known to have a significant orbital moment [30,31]. La_2CoIrO_6 has been recently investigated by Narayanan *et al.* [19]. It shows a ferromagnetic-like transition at 98 K. X-ray magnetic circular dichroism-studies by Kolchinskaya *et al.* revealed that the microscopic magnetic ordering is a canted antiferromagnetic (cAFM) order of the Co sublattice, leading to a net-ferromagnetic moment, to which the $j_{eff} = 1/2$ moments of the Ir^{4+} ions align antiferromagnetically. A contribution of interactions within the Ir-sublattice to the overall magnetism of the compound was not observed [20].

However, when Co^{2+} is replaced by nonmagnetic Zn^{2+} in La_2ZnIrO_6, the Ir-sublattice magnetism can be directly investigated. The ionic radii of the two 3*d* transition metals are very similar ($r_{HS-Co(II)} = 0.745$ Å; $r_{Zn(II)} = 0.74$ Å) [32] and both compounds crystallize in the same space group, monoclinic $P\,2_1/n$. Thus, the change of the Ir-Ir interactions due to lattice changes can be presumed to be negligibly small. Additionally, the equal oxidation state of Co^{2+} and Zn^{2+} means that a change in the oxidation state of iridium, which would lead to deviations from the $j_{eff} = 1/2$ ground state, is not expected.

*m.vogl@ifw-dresden.de
†s.aswartham@ifw-dresden.de

La_2ZnIrO_6 shows a ferromagnetic-like transition at 7.5 K [21]. A recent study by Zhu *et al.* revealed that the underlying magnetic order is cAFM. A second phase transition, which the authors attribute to a change of the canting angle, can be observed in magnetization measurements in low external fields ($H \leqslant 100$ Oe) [22].

Based on the similarity of the crystal structures of La_2ZnIrO_6 and La_2CoIrO_6, a comparison between the magnetism of both compounds leads to the conclusion that Ir-Ir interactions must also be present in La_2CoIrO_6, but are overruled by the stronger Co-Co and Ir-Co interactions. In this paper, we report on the synthesis of $La_2Zn_{1-x}Co_xIrO_6$ and investigate the changes of the magnetic properties when the Co/Zn ratio is varied.

II. EXPERIMENTAL DETAILS

Polycrystalline samples of the parent compounds La_2ZnIrO_6 and La_2CoIrO_6 were prepared by a conventional solid-state reaction. For La_2ZnIrO_6, stoichiometric amounts of La_2O_3, ZnO, and IrO_2 were mixed, ground thoroughly in an agate mortar, and heated to 600 °C overnight. Then the mixture was reground and heated to 1050 °C, dwelled for three days, and later cooled to 500 °C by 15°/h and subsequently cooled to room temperature. Polycrystalline samples of La_2CoIrO_6 were prepared from stoichiometric amounts of La_2O_3, Co_3O_4 and Ir metal powder, which were mixed together, pelletized, and heated to 1200 °C for 50 h with one intermediate grinding. The mixed compounds $La_2Zn_{1-x}Co_xIrO_6$ were prepared from stoichiometric amounts of La_2O_3, ZnO, Co_3O_4, and IrO_2 that were mixed, ground, and pressed to pellets. The pellets were placed in an alumina crucible and heated to 1100 °C with a dwelling time of 60 h, followed by cooling the furnace to 500 °C with a cooling rate of 15 °C/h, and subsequently furnace-cooled to room temperature.

For the structural analysis, x-ray diffraction measurements were carried out in the transmission mode on a StoeStadi-Powder diffractometer with Mo-Kα_1 radiation. Rietveld refinement was performed using the FullProf software package [33,34]. Scanning electron microscopy (SEM) and energy dispersive x-ray spectroscopy (EDXS) were performed on a nanoSEM by FEI. The analysis was carried out on pressed powder pellets. Magnetic measurements were performed using a Quantum Design MPMS-XL SQUID magnetometer. Field-cooled (FC) measurements were done in the cooling mode. Specific-heat measurements were performed using a heat-pulse relaxation method in a Physical Properties Measurement System from Quantum Design.

III. RESULTS AND DISCUSSION

A. Crystal structure

X-ray powder diffraction confirms that all synthesized compounds are obtained phase pure. In particular, no signs of remaining starting materials are visible. Both La_2ZnIrO_6 and La_2CoIrO_6 crystallize in the monoclinic space group $P\,2_1/n$ (space group #14), which is in agreement with earlier reports [19–21]. This space group is indicative for a double perovskite structure with octahedral tilting following the Glazer notation $a^-a^-c^+$ [35].

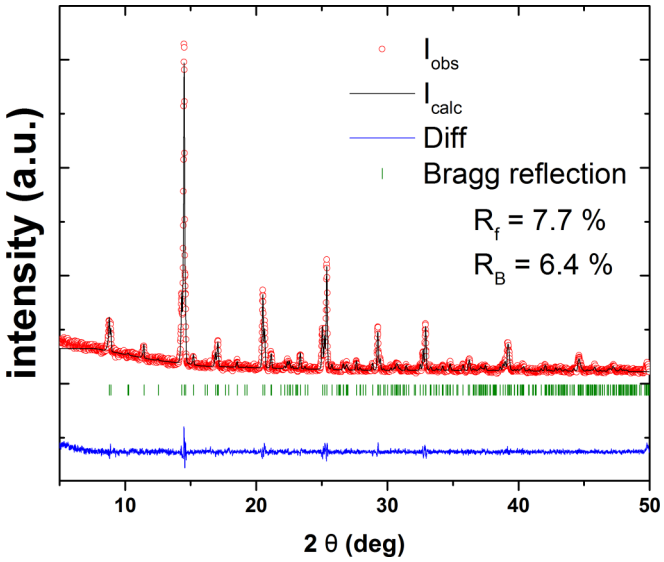

FIG. 1. Selected example illustrating the Rietveld refinement for $La_2Zn_{0.3}Co_{0.7}IrO_6$.

Powder x-ray measurements on the intermediate compounds $La_2Zn_{1-x}Co_xIrO_6$ reveal no major structural changes within the series as the space group remains unchanged. Rietveld refinements were performed for all samples. Figure 1 shows the pattern and refinement of $La_2Zn_{0.3}Co_{0.7}IrO_6$ as a representative example. Refined parameters were lattice constants as well as atomic positions. Anti-site disorder was not investigated as the presence of three different B cations did not allow a distinguished refinement of the site occupancies for all transition metals. All refinements reached a fit quality of $\chi^2 \leqslant 2.2$. It is important to notice that the double perovskite structure remains intact over the whole substitution series. Hence, Ir^{4+} is octahedrally coordinated in all reported compounds, which means that the $j_{\text{eff}} = 1/2$ state, which requires local cubic symmetry, can be assumed to be unaffected by the substitution. Figure 2 shows the evolution of the derived cell parameters. Very small changes of less than 1% are observed, as expected from the almost equal ionic radii of Zn^{2+} and high-spin Co^{2+}. The unit cell volume shows an approximately linear decrease from the Zn parent compound to the Co parent compound following Vegard's law as shown in Fig. 2 (bottom) [36].

B. SEM and EDXS

A compositional analysis was carried out by SEM equipped with EDXS. SEM pictures of all compounds—one example for $x = 0.6$ is shown in Fig. 3—were taken with a secondary electron-detector, showing the topography of the sample, and a backscattered electron-detector (BSED), displaying the chemical contrast. A comparison of the topography and the chemical contrast images confirms the chemical homogeneity of the samples, as color differences in the BSED pictures can be attributed to the rough sample surface. This was also cross-checked by EDXS. A comparison of nominal and measured Zn and Co contents for all compositions is shown in Fig. 4. Small deviations from the nominal composition can be attributed to the rough sample surface, leading to an unequal excitation of

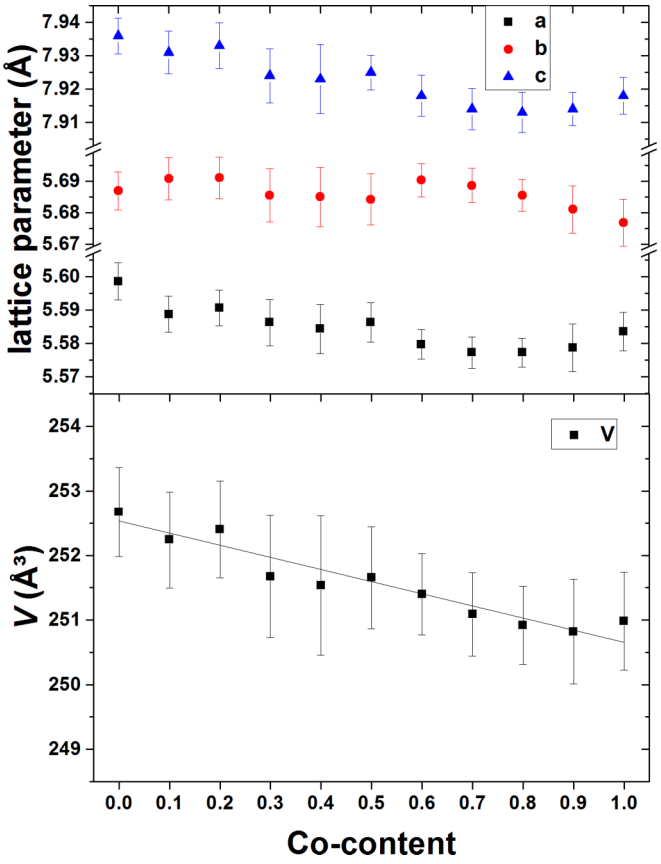

FIG. 2. Evolution of cell parameters a, b, c (top) and cell volume V (bottom). Only small changes in a, b, and c are observed. V decreases approximately linearly towards high Co-contents. The error bars give an estimate on the combined error of measurement and Rietveld refinement. The line serves as guide to the eye.

the elements. Furthermore, the small standard deviations of the values measured at different points of the samples indicate a good homogeneity. In total, the EDXS data point towards full miscibility and a successful formation of the targeted compositions.

C. Magnetic properties

The temperature-dependent magnetization for La_2CoIrO_6 (Fig. 5) is in good agreement with earlier reports [19,20]. In the FC curve, a ferromagnetic-like transition is observed at $T_N \approx$

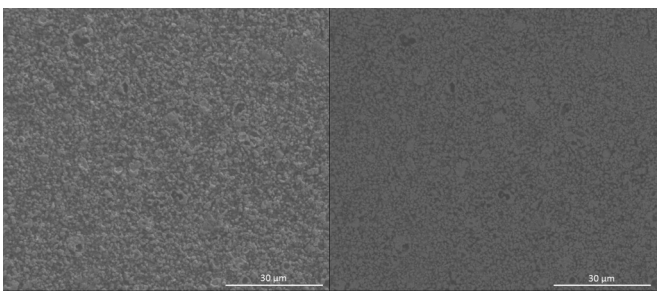

FIG. 3. Topography (left) and chemical contrast (right) images of $La_2Zn_{0.4}Co_{0.6}IrO_6$.

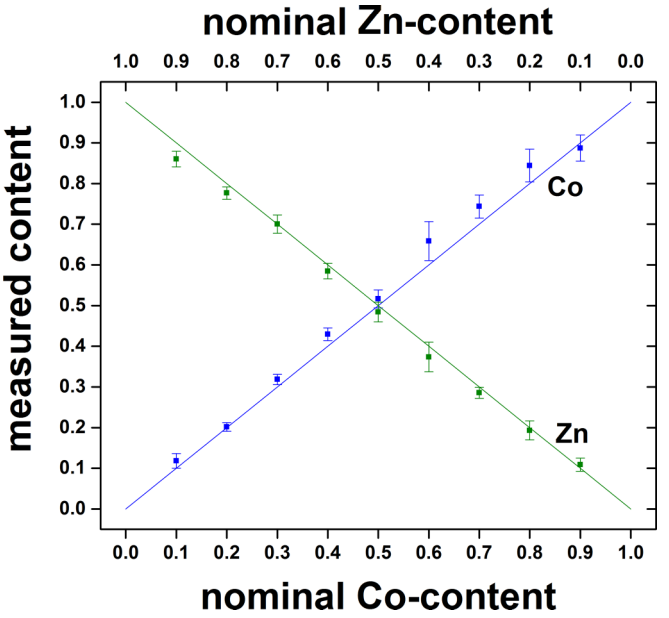

FIG. 4. Confirmation of the gradual Co/Zn ratio change in $La_2Zn_{1-x}Co_xIrO_6$ by EDXS. Error bars indicate the statistical error as a measure of sample homogeneity. The lines show the expected values for the nominal composition.

90 K (all transition temperatures have been determined using the second derivative method, i.e., the transition temperature is defined as the inflection point of the curve). As the Co sublattice reportedly plays the major role in this behavior, dilution of the magnetic *3d* ions by nonmagnetic Zn^{2+} can be expected to strongly influence the magnetic properties of the system. Indeed, in the magnetization data for $La_2Zn_{1-x}Co_xIrO_6$, a shift of T_N towards lower temperatures is observed with decreasing Co content, as shown in Fig. 5. Notably, the shape of the curve remains unchanged for $1 \geqslant x \geqslant 0.3$, indicating that the underlying magnetic order is still similar to the one of La_2CoIrO_6, in the sense that the magnetic ordering of the Co

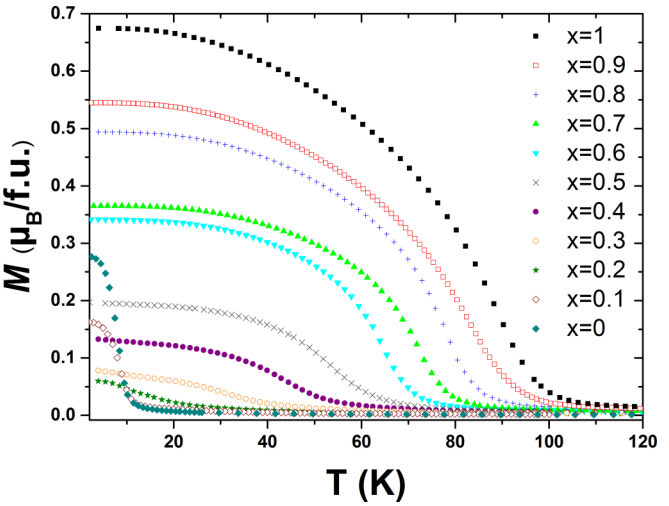

FIG. 5. Field-cooled magnetization of $La_2Zn_{1-x}Co_xIrO_6$ at 0.3 T. The magnetic transition is shifted to lower temperatures as the Co content decreases.

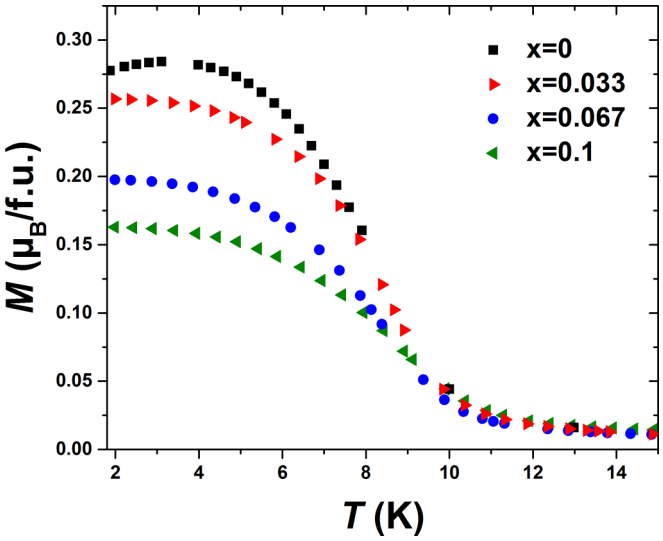

FIG. 6. Field-cooled magnetization for the Zn-rich samples of $La_2Zn_{1-x}Co_xIrO_6$ ($x = 0$, 0.033, 0.067, 0.1) at 0.3 T. A gradual suppression of the magnetic moment with increasing Co content is observed.

sublattice remains dominant even in highly diluted samples with Co contents down to 30%. For $La_2Zn_{0.8}Co_{0.2}IrO_6$, a broad transition is observed. Using the second derivative method to determine the transition temperature leads to $T_N = 9$ K, close to the value known for the Zn parent compound. But an onset in the magnetization curve can already be seen at higher temperatures around 20 K, indicating a remaining contribution of the Co sublattice to the magnetization of this compound. For $La_2Zn_{0.9}Co_{0.1}IrO_6$ and La_2ZnIrO_6, a sharp ferromagnetic-like transition is observed at 7–9 K. This is in agreement with earlier reports for the Zn parent compound [21,22]. Apparently, for $x = 0.1$, the Co sublattice has been so much diluted that its magnetism has almost vanished and is incapable of influencing the Ir-spins. Therefore, the cAFM order known from La_2ZnIrO_6 seems to be already formed in the 10% Co compound.

The magnetization at $T = 2$ K and $\mu_0 H = 0.3$ T decreases over most of the series as the Co content decreases (Fig. 5). Only the step from $x = 0.2$ to $x = 0.1$ and $x = 0$ leads to an increase of the moment. To further investigate the behavior of Co-poor samples, two additional compositions, $La_2Zn_{0.967}Co_{0.033}IrO_6$ and $La_2Zn_{0.933}Co_{0.067}IrO_6$, were synthesized. Figure 6 shows the FC magnetization measurements for $0.1 \geqslant x \geqslant 0$. A general monotonous trend of a decreasing moment with increasing Co-doping is evident. Considering the cAFM ground state of La_2ZnIrO_6, there are two possible explanations for this behavior. A change in the canting angle of the Ir moments, induced by lattice changes upon addition of small amounts of Co, could be the cause for the reduced moments. A similar scenario has been explored in detail by Gatimu *et al.* in $Sr_2Ir_{1-x}Ti_xO_4$, in which structural differences between the two end members, specifically a change of the Ir-O-Ir bond angle, cause significant variations of the Ir-Ir interactions and therefore in the magnetic properties of the materials [37]. However, as no similar structural evolution as a function of substitution can be observed in $La_2Zn_{1-x}Co_xIrO_6$, another explanation has to be considered. It is possible that, similar to the Co-rich samples, an antiparallel alignment of Co and Ir spins is also present in the Zn-rich samples. In this case, inverted roles of the Ir and Co sublattices can be suggested. As the Co sublattice is strongly diluted, the Ir sublattice plays the dominant role, and the isolated Co moments couple to the Ir magnetism antiferromagnetically, reducing the overall magnetic moment of the samples as more Co is added.

For the zero-field-cooled (ZFC) magnetization of $La_2Zn_{1-x}Co_xIrO_6$, three regimes can be observed. The data for $0.9 \geqslant x \geqslant 0.5$ qualitatively resembles the curve shape for La_2CoIrO_6, while the transition temperatures are shifted to lower temperatures [Fig. 7(a)]. This behavior gives another hint that, for $x \geqslant 0.5$, the underlying exchange mechanism resembles the one of La_2CoIrO_6. For $0.4 \geqslant x \geqslant 0.2$, a peak is present in the ZFC curves just like in the Co-rich samples, only further shifted to lower temperatures. Additionally, a cusp appears below 15 K, close to the transition temperature in La_2ZnIrO_6 [Fig. 7(b)]. This can be assumed as a sign of Ir-sublattice interaction, arising from the increased dilution of Co^{2+} by Zn^{2+}, which continuously weakened the Co-Co and Co-Ir interactions, thus, allowing Ir-Ir interactions to leave their mark on the system. Just like in the FC data, the data of $La_2Zn_{0.9}Co_{0.1}IrO_6$ ($x = 0.1$) strongly resembles the parent compound La_2ZnIrO_6 [Fig. 7(b)].

Field-dependent magnetization measurements were performed on the parent compounds as well as on selected intermediate compositions. Our data for the Co parent compound ($x = 1$), taken at 2 K, is in good agreement with earlier literature reports (Fig. 8) [19]. In particular, the steplike feature in the hysteresis, that was observed by Narayanan *et al.*, is confirmed. Narayanan *et al.* attribute this step to a field-dependent change of the canting angle of the noncollinear magnetism in La_2CoIrO_6. As a representative for an intermediate compound with high Co content, the data for $La_2Zn_{0.3}Co_{0.7}IrO_6$ ($x = 0.7$) are additionally shown in Fig. 8. The steplike shape of the hysteresis curve is conserved, once again hinting at a similar magnetic ground state as in La_2CoIrO_6. Additional measurements were performed at 40 K, a temperature well below the Co-sublattice ordering ($T_N \approx 90$ K for $x = 1$; $T_N \approx 73$ K for $x = 0.7$), but above the ordering temperature of the Ir sublattice ($T_N \approx 7.6$ K). As can be observed in the inset of Fig. 8, the step has disappeared. This hints towards a combination of both magnetic sublattices being responsible for the step, as it is only present at temperatures at which both the Co and the Ir sublattice are magnetically active. This finding also implies that the ordering of the Ir sublattice relative to the Co moments in the Co-rich compounds occurs only at low temperatures close to the Ir-sublattice ordering known from La_2ZnIrO_6.

Another indication that the step is caused by the presence of two magnetic sublattices is the fact that no similar feature is known for the Zn parent compound [21,22]. This is confirmed by our data. Likewise, a step-free hysteresis at 2 K is found for Co contents up to $x = 0.3$ (Fig. 9). In addition, the $M(H)$ data confirms the suppression of Ir moments as an effect of Co doping into La_2ZnIrO_6 since a lower moment is measured over the field range up to 7 T, when the Co content is gradually increased from $x = 0$ to $x = 0.3$.

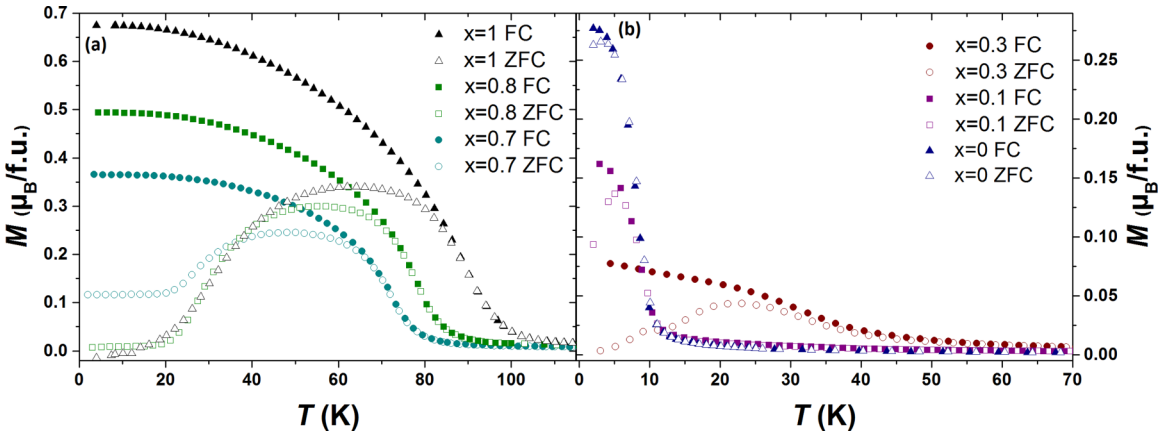

FIG. 7. Comparison of field-cooled (FC) and zero-field-cooled (ZFC) magnetization for the parent compounds La_2CoIrO_6 ($x = 1$) and La_2ZnIrO_6 ($x = 0$) as well as selected intermediate compositions with $x = 0.1, 0.3, 0.7, 0.8$ at 0.3 T. The curves for high Co contents resemble the one for La_2CoIrO_6 [19]. For $x = 0.3$, a kink appears at approximately T = 15 K. The curve for $x = 0.1$ resembles La_2ZnIrO_6.

D. Specific heat

The magnetic behavior of the $La_2Zn_{1-x}Co_xIrO_6$ series was further analyzed by specific-heat measurements as a function of temperature and applied magnetic field. The curves for the parent compounds ($x = 0$ and $x = 1$) are shown in Fig. 10. For La_2ZnIrO_6 ($x = 0$), a magnetic transition occurs at $T_N = 8.7$ K (determined from an entropy-conserving construction), which is gradually suppressed and broadened by the application of a magnetic field [Fig. 10(a)]. The double transition as observed by Zhu *et al.* is much less pronounced for our sample and only detectable for zero field [22]. Still, the behavior is consistent with the one reported by Cao *et al.*, showing a slight shift of the transition to higher temperature in applied magnetic fields, in accordance with the ferromagnetic moment from the cAFM ordering of this material [21]. For the Co-parent compound ($x = 1$), a transition is observed at $T_N \approx 91$ K in zero magnetic field, which is broadened and slightly shifted to higher temperatures by the application of magnetic fields up to 9 T [Fig. 10(b)].

The specific-heat coefficient C_p/T of other representative samples from the series is shown in Fig. 11. All the transition temperatures were determined using an entropy-conserving construction. The samples with the Co content $x = 0.1$ and $x = 0.2$—Fig. 11(a) – show magnetic transitions at $T_N = 10.1$ K and at $T_N = 9.3$ K, respectively, with a suppression and a noticeable shift in applied magnetic fields.

In agreement with the magnetization measurements, the magnetic behavior for these samples still resembles the one for the Zn parent compound. For the $x = 0.6$ sample [Fig. 11(b)], the magnetic transition is detected near 66 K. It is worth noticing that, in all cases, the transition is shifted to higher temperature, showing that the rather strong ferromagnetic component of the cAFM structure is maintained along the full series.

With the aim of calculating the magnetic contribution to the specific heat for the samples with higher Co content ($x = 0.6$ and $x = 1$), the lattice contribution was subtracted from the C_p(T) data. The phononic background was taken from the high temperature data of the Zn compound ($x = 0$, not shown), whose magnetic transition lies well below those of the analyzed $x = 0.6$ and $x = 1$ samples. Due to the differences between the

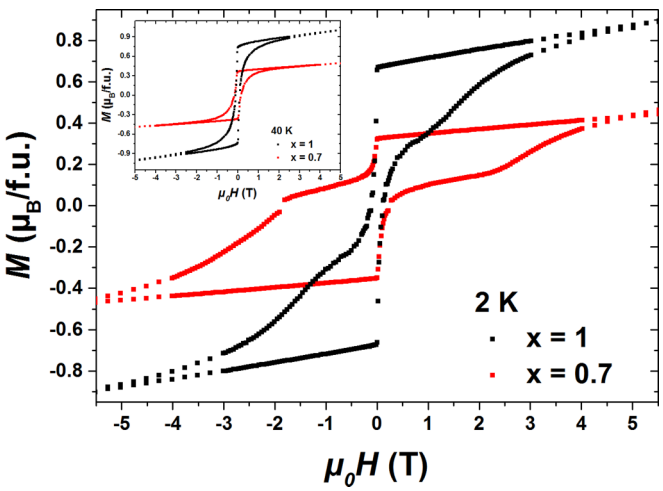

FIG. 8. Field-dependent magnetization of La_2CoIrO_6 and $La_2Zn_{0.3}Co_{0.7}IrO_6$ at 2 K and 40 K (inset). The step in the hysteresis disappears at elevated temperatures.

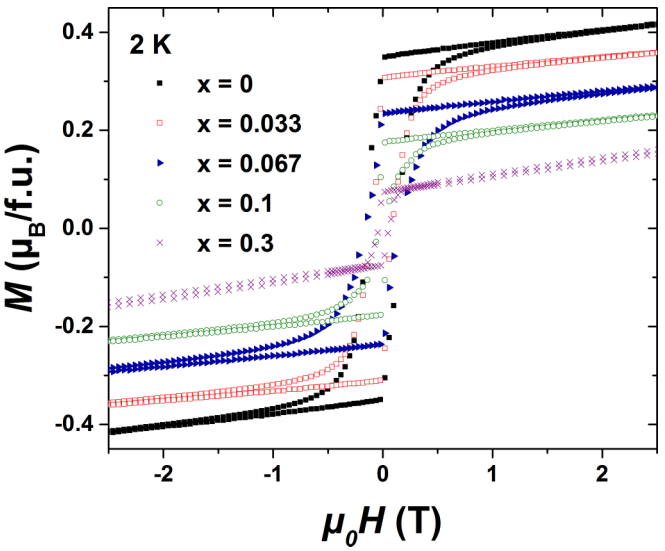

FIG. 9. Field-dependent magnetization for the Zn-rich samples of $La_2Zn_{1-x}Co_xIrO_6$ ($x = 0, 0.033, 0.067, 0.1, 0.3$) at 2 K. Lower μ_B/f.u. values are obtained when the Co content is increased.

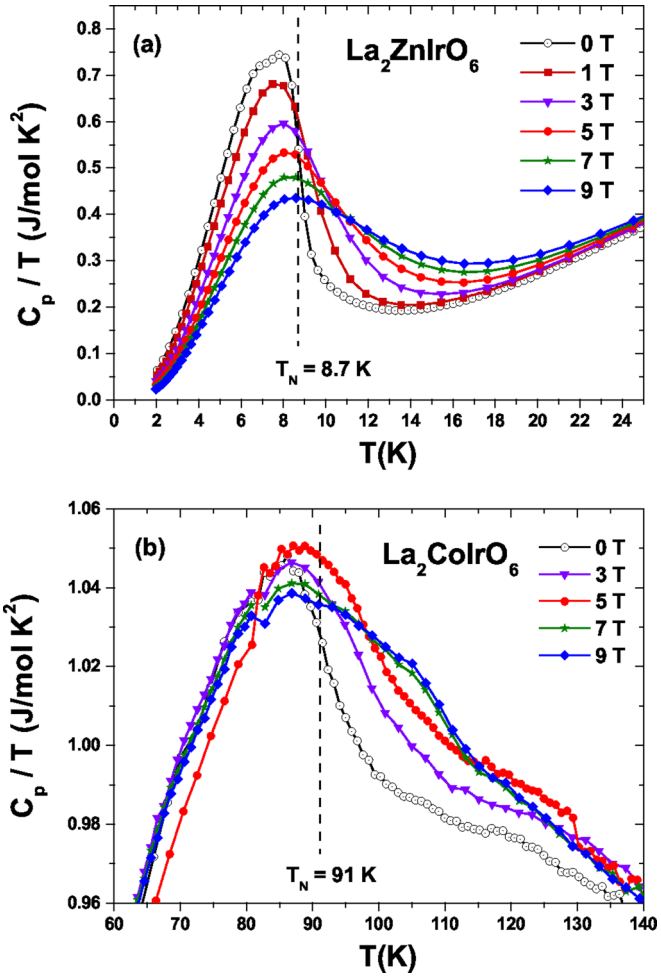

FIG. 10. Temperature dependence of C_p(T)/T under different magnetic fields for (a) La_2ZnIrO_6 and (b) La_2CoIrO_6. The dashed lines indicate the Néel temperature for zero field.

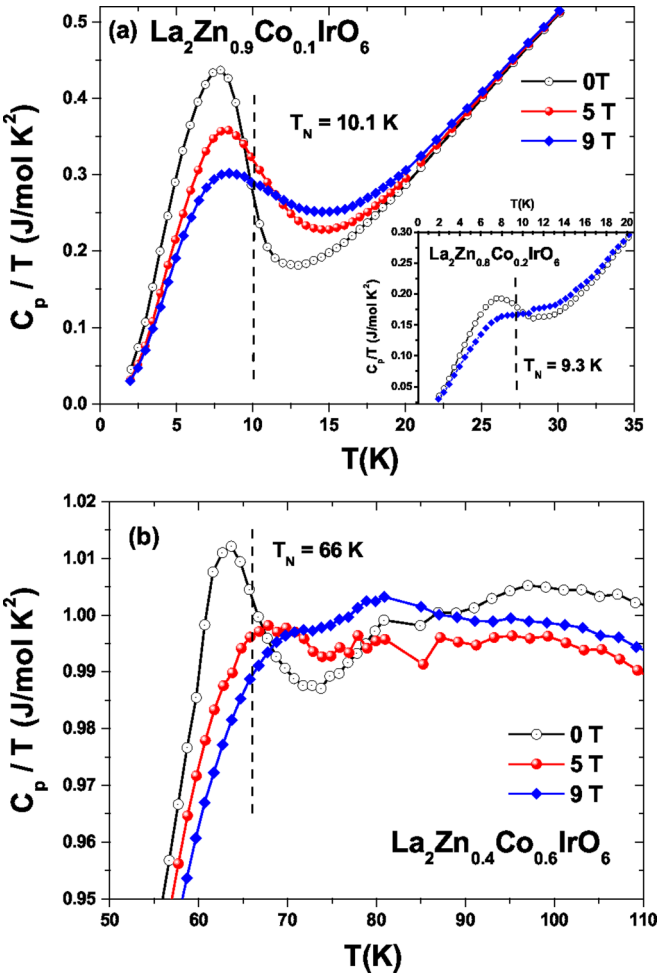

FIG. 11. C_p(T)/T curves in zero field and under the application of magnetic fields for the samples (a) $x = 0.1$, and $x = 0.2$ (inset), (b) $x = 0.6$ (the small discontinuity at 85 K corresponds to a measurement artifact). The dashed lines indicate the Néel temperature for zero field.

mass and volume of Zn and Co, the La_2ZnIrO_6 specific-heat curve was scaled to the Co parent compound by the Lindemann factor 1.005 [18]. Since the difference between the scaling factor for both $x = 1$ and $x = 0.6$ compounds is less than 0.3%, the same factor was taken for both samples. It is known that short-range magnetic correlations are present in La_2ZnIrO_6 up to about 40 K [18]. As a consequence, the analysis could only be performed in the temperature range of 40 K $\leqslant$ T $\leqslant$ 250 K.

The magnetic contribution to the specific heat for both samples is plotted as C_{mag}/T in Fig. 12. A sharp magnetic transition can be observed for both samples as well as some non-negligible magnetic entropy for $T \gg T_N$, which hints towards short-range magnetic correlations up to about 200 K. This is similar to La_2CuIrO_6, where short-range correlations were observed via different methods up to high temperatures [18]. The right scale in Figs. 12(a) and 12(b) shows the magnetic entropy S_{mag}, which was obtained by integrating C_{mag}/T over T. The obtained values of $S_{mag} = 5.8$ J/mol K ($x = 0.6$) and $S_{mag} = 5.9$ J/mol K ($x = 1$) are very close to each other, and at the same time much lower than the expected values, taking into account the $S = 3/2$ from Co^{2+} and $J_{eff} = 1/2$ from Ir^{4+}. For $x = 0.6$, $S_{mag} = 0.6 \cdot R \ln(2S_{Co} + 1) + R \ln(2J_{Ir} + 1) = 12.67$ J/mol K, and for $x = 1$, $S_{mag} = R \ln(2S_{Co} + 1) + R \ln(2J_{Ir} + 1) = 17.28$ J/mol K can be expected theoretically, using a single-ion approach.

Due to magnetic correlations in the low temperature region T < 40 K, for our reference compound La_2ZnIrO_6, some magnetic entropy is missing in the calculated values for $x = 0.6$ and $x = 1$ in our analysis due to the missing phononic background. Still, an approximate extrapolation of the C_{mag}/T curves down to lowest temperature can be performed. We roughly estimate that the missing entropy is of the order of ~1 J/mol K for the $x = 0.6$ sample and of ~0.7 J/mol K for the Co parent compound, resulting in $S_{mag} = 6.8$ J/mol K and $S_{mag} = 6.6$ J/mol K, respectively.

Despite the limits of our phononic background, the entropy reduction in both systems is evident. A probable scenario is the existence of a large SOC (from Ir) and a large orbital contribution/reduction (from Co) that the system experiences. On the other hand, the magnetization measurements of the samples with high Co content clearly indicated the comparably small Ir-Ir interactions and, thus, magnetic contributions, which are overruled by the stronger Co contribution. Thus, the observed small values for the entropy could reflect the

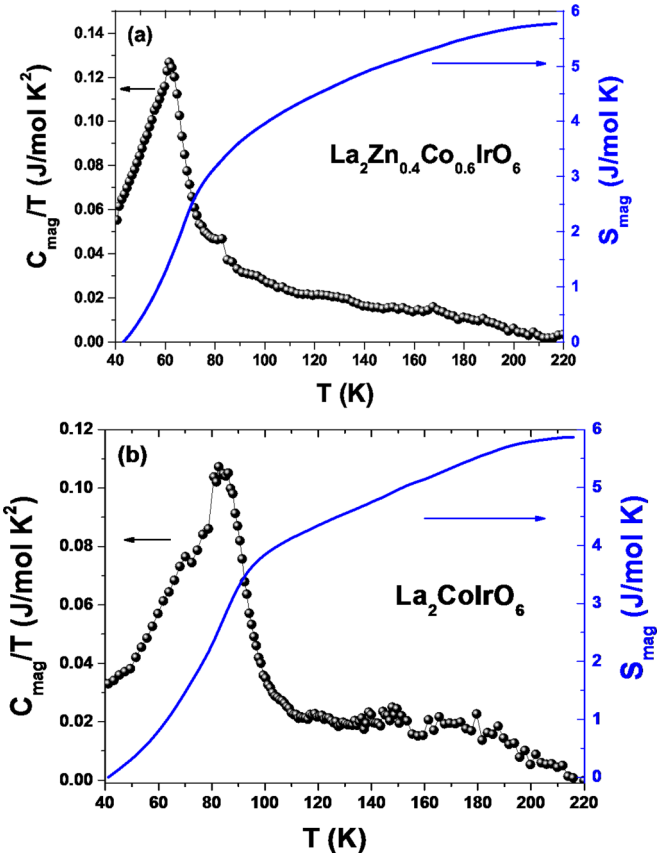

FIG. 12. Zero-field magnetic specific heat of the samples with Co content (a) $x = 0.6$ and (b) $x = 1$, plotted as C_{mag}/T vs T (left scale) and the calculated magnetic entropy $S_{mag}(T)$ (right scale) in the temperature range 40 K $\leqslant$ T $\leqslant$ 220 K. The kink at 85 K is due to the same artifact observed in Fig. 11(b).

dominating Co^{2+} entropy, which would be even more reduced in combination with the first proposed scenario.

IV. CONCLUSION

Polycrystalline samples of $La_2Zn_{1-x}Co_xIrO_6$ were successfully synthesized. While structural changes are minor, a strong dependence of the magnetic transition temperature on the Co/Zn ratio was observed. The system shows non trivial magnetism and a strong interplay of the Ir and Co sublattices can be assumed. Both field-cooled and ZFC magnetization measurements show signs of a transition from a 3*d* sublattice dominated magnetic order to an independent order of the 5*d* sublattice for $x \leqslant 0.2$, in line with the fact that small amounts of Co doping into La_2ZnIrO_6 were found to suppress the magnetic moment of the material. Specific-heat studies on selected compounds confirm the transition temperatures derived from the magnetization measurements. The calculation of the magnetic entropy reveals an entropy reduction, which points towards a large SOC and orbital contributions.

Taking the transition temperatures obtained from both the magnetization measurements and the specific-heat studies, the phase diagram of $La_2Zn_{1-x}Co_xIrO_6$ has been mapped out, as shown in Fig. 13. With lower Co contents, the paramagnetic (PM) phase remains stable down to progressively lower temperatures before the system undergoes the transition towards the cAFM state.

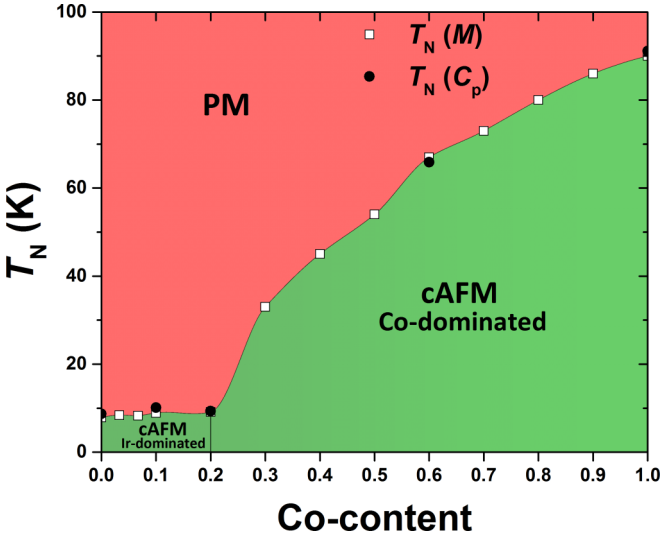

FIG. 13. Phase diagram of $La_2Zn_{1-x}Co_xIrO_6$ illustrating the shift of the transition temperature between paramagnetic (PM) and canted antiferromagnetic (cAFM) phases. Open squares represent transition temperatures from magnetization measurements. Filled circles represent transition temperatures from the specific-heat study. The additions Co-dominated and Ir-dominated refer to cAFM orders primarily caused by Co-Co or Ir-Ir interactions, respectively.

To fully understand the magnetic ground states present in the intermediate compositions of $La_2Zn_{1-x}Co_xIrO_6$, further experimental and theoretical work is needed. A neutron-powder diffraction study similar to the one done for La_2CoIrO_6 by Narayanan *et al.* in Ref. [19] could, for example, shed light on the evolution of the canting angle in the Co sublattice as a function of dilution by Zn, as well as help to understand the role of the Co moments in the suppression of the magnetism in the Zn-rich samples. Detailed x-ray spectroscopy methods like resonant inelastic x-ray scattering could also reveal more information on the individual orderings of the two magnetic sublattices and thus deepen the understanding of the interactions between the 3*d* and the 5*d* magnetic ions.

Theoretical studies on the nature of magnetic exchange interactions between 3*d* and 5*d* magnetic ions in double perovskites have so far been done on osmates and rhenates [38–40]. For iridates, the focus has been on double perovskites with with Ir(V) states [41,42], as well as the Ir(IV) compounds La_2ZnIrO_6 and La_2MgIrO_6, which possess a geometrically frustrated fcc lattice of iridium as the only magnetic ion [43]. Further theoretical work on Ir(IV)-based double perovskites with two magnetic sublattices could shed more light on the intriguing phenomena observed experimentally in La_2CoIrO_6, as well as La_2CuIrO_6 and La_2NiIrO_6 [16–18].

ACKNOWLEDGMENTS

This paper was supported by the Deutsche Forschungsgemeinschaft within Project No. B01 of the SFB 1143, and Grant No. WO 1532/3-2. We acknowledge C. G. F. Blum, S. Gaß, and S. Müller-Litvanyi for technical support.

[1] B. J. Kim, H. Jin, S. J. Moon, J.-Y. Kim, B.-G. Park, C. S. Leem, J. Yu, T. W. Noh, C. Kim, S.-J. Oh, J.-H. Park, V. Durairaj, G. Cao, and E. Rotenberg, Phys. Rev. Lett. **101**, 076402 (2008).

[2] D. Pesin and L. Balents, Nat. Phys. **6**, 376 (2010).

[3] W. Witczak-Krempa, G. Chen, Y. B. Kim, and L. Balents, Annu. Rev. Condens. Matter Phys. **5**, 57 (2014).

[4] Y. Singh, S. Manni, J. Reuther, T. Berlijn, R. Thomale, W. Ku, S. Trebst, and P. Gegenwart, Phys. Rev. Lett. **108**, 127203 (2012).

[5] X. Wan, A. M. Turner, A. Vishwanath, and S. Y. Savrasov, Phys. Rev. B **83**, 205101 (2011).

[6] B.-J. Yang and Y. B. Kim, Phys. Rev. B **82**, 085111 (2010).

[7] Y. Du and X. Wan, Comput. Mater. Sci. **112**, 416 (2016).

[8] J. Chaloupka, G. Jackeli, and G. Khaliullin, Phys. Rev. Lett. **105**, 027204 (2010).

[9] L. Balents, Nature **464**, 199 (2010).

[10] F. Wang and T. Senthil, Phys. Rev. Lett. **106**, 136402 (2011).

[11] C. Moure and O. Pena, Prog. Solid State Chem. **43**, 123 (2015).

[12] H. S. Bhatti, S. T. Hussain, F. A. Khan, and S. Hussain, Appl. Surf. Sci. **367**, 291 (2016).

[13] M. Guennou, M. Viret, and J. Kreisel, C. R. Phys. **16**, 182 (2015).

[14] A. K. Kundu, M. M. Seikh, and P. Nautiyal, J. Magn. Magn. Mater. **378**, 506 (2015).

[15] S. Vasala and M. Karppinen, Prog. Solid State Chem. **43**, 1 (2015).

[16] A. V. Powell, J. G. Gore, and P. D. Battle, J. Alloys Compd. **201**, 73 (1993).

[17] R. C. Currie, J. F. Vente, E. Frikkee, and D. J. W. Ijdo, J. Solid State Chem. **116**, 199 (1995).

[18] K. Manna, R. Sarkar, S. Fuchs, Y. A. Onykiienko, A. K. Bera, G. A. Cansever, S. Kamusella, A. Maljuk, C. G. F. Blum, L. T. Corredor, A. U. B. Wolter, S. M. Yusuf, M. Frontzek, L. Keller, M. Iakovleva, E. Vavilova, H.-J. Grafe, V. Kataev, H.-H. Klauss, D. S. Inosov, S. Wurmehl, and B. Büchner, Phys. Rev. B **94**, 144437 (2016).

[19] N. Narayanan, D. Mikhailova, A. Senyshyn, D. M. Trots, R. Laskowski, P. Blaha, K. Schwarz, H. Fuess, and H. Ehrenberg, Phys. Rev. B **82**, 024403 (2010).

[20] A. Kolchinskaya, P. Komissinskiy, M. B. Yazdi, M. Vafaee, D. Mikhailova, N. Narayanan, H. Ehrenberg, F. Wilhelm, A. Rogalev, and L. Alff, Phys. Rev. B **85**, 224422 (2012).

[21] G. Cao, A. Subedi, S. Calder, J.-Q. Yan, J. Yi, Z. Gai, L. Poudel, D. J. Singh, M. D. Lumsden, A. D. Christianson, B. C. Sales, and D. Mandrus, Phys. Rev. B **87**, 155136 (2013).

[22] W. K. Zhu, C.-K. Lu, W. Tong, J. M. Wang, H. D. Zhou, and S. X. Zhang, Phys. Rev. B **91**, 144408 (2015).

[23] R. Morrow, J. R. Soliz, A. J. Hauser, J. C. Gallagher, M. A. Susner, M. D. Sumption, A. A. Aczel, J. Yan, F. Yang, and P. M. Woodward, J. Solid State Chem. **238**, 46 (2016).

[24] A. K. Paul, A. Sarapulova, P. Adler, M. Reehuis, S. Kanungo, D. Mikhailova, W. Schnelle, Z. Hu, C. Kuo, V. Siruguri, S. Rayaprol, Y. Soo, B. Yan, C. Felser, L. H. Tjeng, and M. Jansen, Z. Anorg. Allg. Chem. **641**, 197 (2015).

[25] A. E. Taylor, R. Morrow, D. J. Singh, S. Calder, M. D. Lumsden, P. M. Woodward, and A. D. Christianson, Phys. Rev. B **91**, 100406(R) (2015).

[26] P. M. Woodward, Acta Cryst. **B53**, 32 (1997).

[27] P. M. Woodward, Acta Cryst. **B53**, 44 (1997).

[28] I. Dzyaloshinskii, J. Phys. Chem. Solids **4**, 241 (1958).

[29] T. Moriya, Phys. Rev. **120**, 91 (1960).

[30] W. Neubeck, C. Vettier, F. de Bergevin, F. Yakhou, D. Mannix, L. Ranno, and T. Chatterji, J. Phys. Chem. Solids **62**, 2173 (2001).

[31] R. J. Radwanski and Z. Ropka, Physica B **345**, 107 (2004).

[32] R. D. Shannon and C. T. Prewitt, Acta Cryst. **B25**, 925 (1969).

[33] H. M. Rietveld, J. Appl. Cryst. **2**, 65 (1969).

[34] T. Roisnel and J. Rodriguez-Carvajal, Mater. Sci. Forum **378**, 118 (2001).

[35] A. M. Glazer, Acta Cryst. B **28**, 3384 (1972).

[36] L. Vegard, Z. Phys. **5**, 17 (1921).

[37] A. J. Gatimu, R. Berthelot, S. Muir, A. W. Sleight, and M. A. Subramanian, J. Solid State Chem. **190**, 257 (2012).

[38] K. W. Plumb, A. M. Cook, J. P. Clancy, A. I. Kolesnikov, B. C. Jeon, T. W. Noh, A. Paramekanti, and Y.-J. Kim, Phys. Rev. B **87**, 184412 (2013).

[39] S. Kanungo, B. Yan, C. Felser, and M. Jansen, Phys. Rev. B **93**, 161116(R) (2016).

[40] P. Sanyal, Phys. Rev. B **89**, 115129 (2014).

[41] X. Ou, Z. Li, F. Fan, H. Wang, and H. Wu, Sci. Rep. **4**, 7542 (2014).

[42] O. El Rhazouani, M. El Khatabi, A. Slassi, A. Benyoussef, and A. El Kenz, Phys. Lett. A **380**, 4075 (2016).

[43] A. M. Cook, S. Matern, C. Hickey, A. A. Aczel, and A. Paramekanti, Phys. Rev. B **92**, 020417(R) (2015).